

# Boosting Content Based Image Retrieval Performance Through Integration of Parametric & Nonparametric Approaches

Soumya Prakash Rana<sup>a</sup>, Maitreyee Dey<sup>a</sup>, Patrick Siarry<sup>b</sup>

<sup>a</sup>London South Bank University, 103 Borough Rd, London SE1 0AA, United Kingdom

<sup>b</sup>University of Paris-Est Creteil, 61 Avenue du General de Gaulle, 94000 Creteil, Paris, France

---

## Abstract

The collection of digital images is growing at ever-increasing rate which rises the interest of mining the embedded information. The appropriate representation of an image is inconceivable by a single feature. Thus, the research addresses that point for content based image retrieval (CBIR) by fusing parametric color and shape features with nonparametric texture feature. The color moments, and moment invariants which are parametric methods and applied to describe color distribution and shapes of an image. The nonparametric ranklet transformation is performed to narrate the texture features. Experimentally these parametric and nonparametric features are integrated to propose a robust and effective algorithm. The proposed work is compared with seven existing techniques by determining statistical metrics across five image databases. Finally, a hypothesis test is carried out to establish the significance of the proposed work which, infers evaluated precision and recall values are true and accepted for the all image database.

*Keywords:* CBIR, Color Moments, Ranklet Transform, Nonparametric Statistics, Moment Invariants, Hypothesis Test

---

## 1. Introduction

1 With the explosion of digital technologies and greater storage capabilities, vast volumes of  
2 digital media now exist in various fields like, multimedia and spatial information system [1],  
3 medical image [2], time series data analysis [3], compression techniques [4]. When a required  
4 image is being located, normally employed methods are via keyword indexing or by sim-  
5 ply browsing, which can be very time consuming and may not result in the exact image  
6 sought. This necessitate the development of an efficient algorithm for managing, indexing  
7 and searching these large image libraries. There are two types of image searching techniques,  
8 text-based image retrieval (TBIR) and content-based image retrieval (CBIR). TBIR relies on  
9 the manual search by keyword matching of existing image titles. The outcomes depend upon  
10 the human labelling which leads to irrelevant results and wastage of time [5] whereas, CBIR  
11 technique relies on low-level image features and reduces human labour drastically. However,  
12 these features are failed to represent a required image.  
13  
14

---

*Email addresses:* [ranas9@lsbu.ac.uk](mailto:ranas9@lsbu.ac.uk) (Soumya Prakash Rana), [deym@lsbu.ac.uk](mailto:deym@lsbu.ac.uk) (Maitreyee Dey),  
[siarry@u-pec.fr](mailto:siarry@u-pec.fr) (Patrick Siarry)

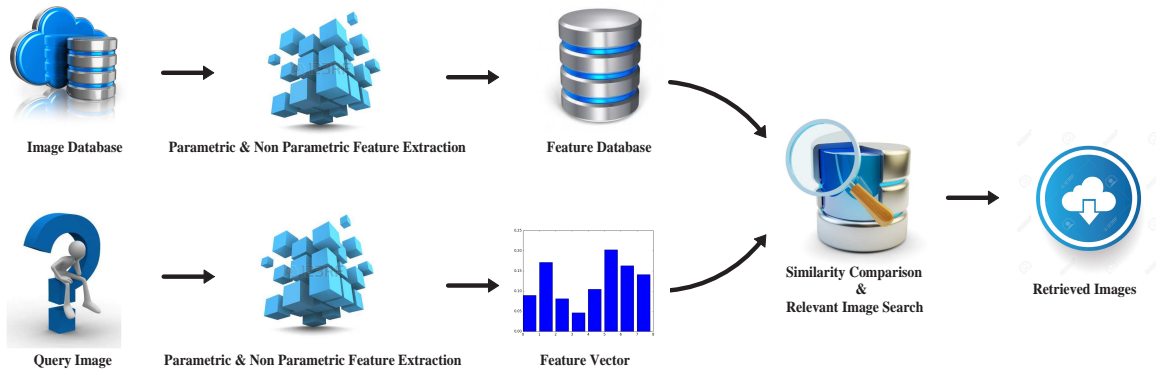


Figure 1: CBIR system structure.

15 CBIR is an image searching method from large image database depending upon extracted  
 16 features by the visual descriptors. Here, user asks for an image and CBIR system searches for  
 17 relevant images based on extracted features from stored images of the databases. This system  
 18 structure of CBIR is described in Figure 1 where, user makes query, then visual content de-  
 19 scriptor or feature extractor extracts low level features (e.g., color, texture, and shape) from  
 20 the query image. Thus, CBIR is also known as feature based image retrieval (FBIR) [6, 7].  
 21 Then the distance is measured between query or example image with the feature vectors  
 22 of stored images to find out the similarity and retrieve images on a suitable match. In  
 23 some cases, researchers proposed region based image retrieval (RBIR), an extended version  
 24 of CBIR where, images are segmented into different regions and features are extracted from  
 25 each regions to represent an image. Unfortunately, the similarity measurement cost is very  
 26 high in this case which, restricts RBIR from wide acceptance [8]. Therefore, the performance  
 27 of a CBIR system heavily depends upon the low-level image processing or the extraction of  
 28 fundamental image primitives. These primitives are derived to represent the images in such  
 29 a way, that could express the query of a human mind properly through the numerical form.  
 30 This is a challenging task over the decades for the researchers of CBIR field to express human  
 31 concepts through features for mining the other similar images. Hence, the minimization of the  
 32 gap of similarity between an example image and the retrieved images by the CBIR method is  
 33 the main goal where, it can help user in various domains such as, image searching, browsing,  
 34 remote sensing, crime prevention, publishing, medicine, architecture, historical research, etc.  
 35

### 36 1.1. Related Work

37 CBIR techniques most commonly employ visual color, texture and shape information. These  
 38 existing feature extraction methods are relied on global and local features. Global features  
 39 cover the whole image as visual content, whereas local feature based algorithms focus on  
 40 key points or selected regions of a whole image. Several algorithms exist on global and local  
 41 features extraction. Color is a wavelength-dependent perception [9] which has evolved as a  
 42 widely used visual character for image retrieval and object recognition. Color histogram is  
 43 a well known color descriptor which is invariant to orientation and scale. These properties  
 44 make it a powerful image classification technique. Image retrievals based on this method  
 45 were easy to implement and commonly used in CBIR fields. However, color histogram faces

46 difficulties when, characterizing images with spatial structures. Subsequently, a number of  
47 color descriptors aimed at exploiting spatial information have been proposed. Those are  
48 mainly compact color moments, color coherence vector, and color autocorrelograms [10]. For  
49 example, in the MPEG-7 standard, color descriptors comprise histograms such as, color lay-  
50 out descriptor, dominant color descriptor, and scalable color descriptor [11, 12]. An indexed  
51 and encoded explanation of color information is utilized for improvement of CBIR results. It  
52 actually discards unimportant colors and keeps important color information to make indexed  
53 color histogram, which is further represented by golomb-rise (GR) encoding [13].

54  
55 One of the pivotal characteristics of an image is texture which is frequently employed in  
56 CBIR systems. Texture analysis uses various algorithms e.g., gray level co-occurrence matri-  
57 ces (GLCM) [14], tamura texture feature [15], the markov random field (MRF) model [16],  
58 gabor filtering [17], and local binary patterns (LBP) [18]. Three types of texture descriptor are  
59 utilized in MPEG-7 standard; i.e., edge histogram descriptor, homogeneous texture descrip-  
60 tor, texture and browsing descriptor [11, 12]. Generally, these texture features are combined  
61 with color features to improve discrimination power and to enhance retrieval performance.  
62 In most of the cases, texture extraction algorithms combine color and gray-level texture fea-  
63 tures such as, multi-texton histogram [19], texton co-occurrences matrix [20], micro-structure  
64 description [21], and color edge co-occurrence histogram [22].

65  
66 Shape features are also additionally applied in many research work like color and texture  
67 features. This simply works on the fact that humans can distinguish objects solely by their  
68 shapes. Classical methods to describe shape features include the use of moment invariants,  
69 fourier transform coefficients, edge curvature and arc length [23, 24]. MPEG-7 employs three  
70 shape descriptors for object-based image retrieval such as, 3D shape descriptor, region-based  
71 shapes derived from zernike moments, and the curvature scale space (CSS) descriptor [12].  
72 In addition, local image feature extraction (LIFE) is also gaining the attention. One popular  
73 LIFE technique is scale invariant feature transform (SIFT) [25], which can tolerate some  
74 illumination change, perspective distortion, and transformation. It is also quite robust to oc-  
75 clusion issues. Another well known LIFE is the bag-of-visual words, which are derived from  
76 local features such as, key points and salient patches. This was actually proposed for object  
77 recognition and scene categorization [26]. Essentially, this algorithm is highly motivated by  
78 retrieval methods. This method has some limitations e.g., it heavily relies on computation  
79 power since it uses clustering techniques. Also, insufficient semantic information, text ambi-  
80 guity, and long feature lengths makes it deficient. In practice, the classification accuracy of  
81 text words is far superior than visual words.

82  
83 Apart from the individual use of color, texture, and shape, high number of CBIR works rely  
84 on multi-feature fusion to have better performance. Distribution of Color Ton (DCTon) [27] is  
85 a hybrid CBIR framework to extract the inter class features using color distribution with the  
86 help of dual tree complex wavelet transformation and singular value decomposition (SVD).  
87 It represents both color and texture information. Global correlation descriptor (GCD) [28]  
88 is proposed to extract color and texture features to enhance image retrieval performance. It  
89 has two sub-parts, global correlation vector (GCV) and directional global correlation vector  
90 (DGCV) which are using the advantages of histogram statistics and structure element correla-

91 tion (SEC) to express color and texture features respectively. Multi-trend structure descriptor  
92 (MTSD) [29], describes color, shape, texture, and local spatial structure information to define  
93 an image in CBIR. It uses local structures of images to explore correlation between pixels.  
94 Color, edge orientation, and intensity mapping are considered to build the model. Srivastava  
95 and Khare [30] proposed a method using discrete wavelet transform (DWT), and local binary  
96 pattern (LBP) with legendre moments (LM) for refining the retrieval performance where, im-  
97 ages are converted to gray scale for different levels of decomposition and then LBP extracts  
98 texture features from decomposed elements. A hybrid textual-visual relevance is used in [31]  
99 which, mines image tags, combines textural relevance and visual relevance for image retrieval.  
100 It is actually followed by correction of missing tags, capturing user’s semantic cognition and  
101 finally a probability distribution on the permutations of tags are executed. Finally, instead  
102 of early fusion, a ranking aggregation strategy is acquired to sew up textual relevance and  
103 visual relevance seamlessly.

104

### 105 *1.2. Scope & contributions*

106 Though, the aforementioned CBIR literature is quite strong still it needs improved compu-  
107 tation due to the recent advancement. This includes availability of vast image database, fast  
108 computation for quick and relevant image retrieval. Thus, the proposed CBIR study is moti-  
109 vated by the fact of appropriate image retrieval for user search. Existing research is focused  
110 on: parametric features, nonparametric features, fusion of different parametric features, and  
111 fusion of different nonparametric features. The parametric approaches derive features by  
112 making assumption of pixel distribution where, nonparametric approach doesn’t make as-  
113 sumption of pixel distribution and determines ranking from available numerical values [32].  
114 Hence, a CBIR system which, employs only parametric color features for image retrieval faces  
115 problem to characterize an image containing more significant texture and shape information.  
116 In the same way, CBIR systems which only use nonparametric shape extraction method to  
117 describe an image are failed to describe color and texture information. Therefore, a hybrid  
118 CBIR method is proposed here that intends to depict an image through all three kinds of low  
119 level image features (color, texture, and shape) with minimal information lose which would be  
120 beneficial for this domain. This work is integrated color moments (parametric method), ran-  
121 klet transformation (nonparametric method), and moment invariants (parametric method)  
122 to develop an efficient and robust CRM method. The contributions to the work using CRM  
123 are as follows:

- 124 I. Color features are determined through the CIE Lab color space which approximates  
125 the human vision better than RGB color model. Then, the distribution of colors in an  
126 image is measured by color moments for characterization of color features. The main  
127 focus of this research is the ranklet transformation which is nonparametric statistical  
128 method for texture analysis based on nonlinear rank based filtering technique, provides  
129 alternative series of measurements that requires very limited assumptions to be made  
130 about the data points. This is invariant in nature towards transformations (bright-  
131 ness, contrast changes and gamma correction). Also, moment invariants are executed  
132 for shape analysis which, is weighted average (moment) of the image pixel’s intensities  
133 of object in an image. Subsequently, these three parametric and nonparametric fea-

134 tures are concatenated for making a better feature vector of an image which is able to  
135 represent all low-level characteristics present there.

136 II. After, enhancing the feature extraction process, different similarity measurements are  
137 evaluated to find out suitable similarity method and enlarge the number of relevant  
138 images for a search. Four distinct distance algorithms: Chi-squared test or  $X^2$  statistics,  
139 Manhattan, Euclidean, and Canberra distance are investigated and found Euclidean  
140 distance outperforms among them with better precision and recall. The Euclidean  
141 measure is executed with the enhanced features to retrieve images from five different  
142 image databases by applying three different frame sizes (10, 12, 15).

143 III. The proposed CRM model is also compared with seven different existing CBIR tech-  
144 niques: color difference histogram (CDH) [33], edge histogram descriptor (EHD) [34],  
145 multi-texton histogram (MTH) [19], color auto correlogram (CAC) [10], distribution of  
146 color ton (DCTon) [27], golomb-rice (GR) coding based indexed histogram [13], and  
147 local binary pattern (LBP) based method with the combination of discrete wavelet  
148 transformation (DWT) and legendre moments (LM) which is denoted as (LDM) [30].

149 IV. Statistical measurements are performed to validate the work and show the performance  
150 of the proposed CRM are superior than other compared methods. In addition, a hypoth-  
151 esis test is performed and a thorough analysis is accomplished to exhibit the potentiality  
152 of this study.

153 This article is organized as follows: Section 2 gives the detailed description about the pro-  
154 posed CRM method which includes the feature extraction procedure (Section 2.1), similarity  
155 measurement (Section 2.2), performance evaluation (Section 2.3), and hypothesis test (Sec-  
156 tion 2.4). Afterthat, experiment and result analysis are discussed in Section 3 with parameters  
157 are fitted in the proposed model (Section 3.1), data details (Section 3.2), retrieval performance  
158 (Section 3.3), and result validation (Section 3.4). Finally, conclusion is presented in Section 4.

## 159 2. Proposed Method

160 Proposed work is divided into two phases: online and offline along with four sub-stages  
161 such as, feature extraction, similarity measure, performance evaluation, and hypothesis test.  
162 Figure 2 shows the flow of this work and connection between each parts. Initially, the color,  
163 texture, and shape features are extracted from all images of a database to create the database  
164 of feature vectors using CRM method and stored in offline phase. In the online phase, when  
165 user makes a query image to retrieve relevant images then, CRM algorithm is performed to  
166 derive features to form feature vector of the query image. Then, the feature vector of the  
167 query image is compared with the stored feature vectors by the help of similarity tolerance to  
168 fetch the relevant images for the user. Thereafter, the statistical metrics are determined over  
169 the retrieved images to check the ability of the proposed CRM method for searching relevant  
170 images. In addition, the hypothesis test is performed to assure the ability of the work.

### 171 2.1. Feature Extraction

172 The feature extraction technique of CRM are detailed in this section. Initially, this process  
173 is started with an image and applied for all stored images as well as the query for deriving  
174 feature values which are informative and non-redundant for better human interpretation.

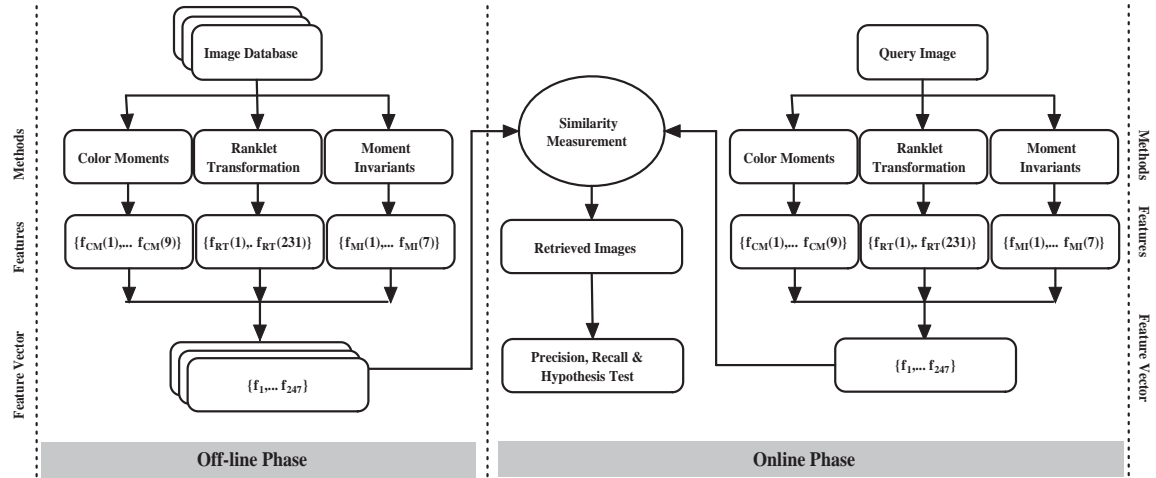


Figure 2: Flow diagram of proposed CBIR system.

### 175 2.1.1. Color Moments

176 Color is extremely used feature for image retrieval techniques [35]. Before selecting an appropriate color description, selection of color space is important and needs to choose a color model for color feature extraction process. Generally databases consider images in RGB format. However, this format contains highly redundant and correlated intensity values which degrade the efficiency of an algorithm. Thus, the proposed algorithm adapted CIE Lab color space for pulling out the color feature because of these pros and cons of RGB color model. It is a 3-axis color system with dimension  $L$  for lightness,  $a$  and,  $b$  for the color dimensions. The Lab color space includes all the colors of spectrum, as well as the colors of outside human perception. This is the most exact means of representing color and this is device independent color space. Scale and rotation invariant are most effective properties of this method where, first three color moments i.e., mean, variance, skewness are used as features in images retrieval. These are proved as effective and efficient features to represent color distribution of an image [36]. Color moments are defined below in (1) to (3),

$$189 \alpha_i = \frac{1}{N} \sum_{j=1}^n f_{ij} \quad (1)$$

$$190 \beta_i = \left( \frac{1}{N} \sum_{j=1}^n (f_{ij} - \alpha_i)^2 \right)^{\frac{1}{2}} \quad (2)$$

$$\gamma_i = \left( \frac{1}{N} \sum_{j=1}^n (f_{ij} - \alpha_i)^3 \right)^{\frac{1}{3}} \quad (3)$$

191 where,  $\alpha_i$ ,  $\beta_i$ ,  $\gamma_i$  indicate mean, variance, and skewness, respectively;  $f_{ij}$  is the value of  $i$ -th color component of the image pixel  $j$ , and  $N$  is the number of pixel in the image. Color moments are calculated for each color channel (L, a, b) of an image. Therefore, 9 distinct color features are generated from color moments for a single image. The execution steps are listed in Algorithm 1.

---

**Algorithm 1** Pseudo code for color moments

---

**Require:** all the color values are in *CIE L \* a \* b* color space

*CIE L \* a \* b* image function =  $f(x, y)$

**for all** *Color components* =  $L, a, b$  **do**

**for all**  $x = 1$  to *Number of rows in image* **do**

**for all**  $y = 1$  to *Number of columns in image* **do**

            Calculate  $\alpha, \beta, \gamma$

$\Leftarrow$  using the Eq. 1, 2, 3

**end for**

**end for**

**end for**

**Return,** *Feature vector*

---

196 *2.1.2. Ranklet Transformation*

197 Texture analysis of an image is the salient part of image description. A texture is a  
198 repeating appearance of particular pattern or intensities in an image which, draws the details  
199 about spatial alignment of these elements. There are two ways to analyze image texture i.e.,  
200 structured and statistical approach. Structured approach considers the repetitive relation-  
201 ship of primitive texels whereas, texture is being considered as quantitative measure of the  
202 intensity arrangement in statistical approach. Here, proposed CRM method used ranklet  
203 transformation [37] to extract texture features. This is a non-parametric, multi-resolution  
204 and orientation selective algorithms that adopts the wavelet style. Ranklet coefficients are  
205 calculated for different resolution and orientation based on non-parametric statistics which  
206 deals with relative order of pixels instead of their intensity values. These rank based nonlin-  
207 ear filtering drops high spatial frequencies associated with noise, shifts the mean intensity in  
208 the direction of skewness, and preserves the shape of edges where no new intensity values are  
209 generated during this phase [38]. Here, texture feature extraction consists of two steps, one  
210 preprocessing step using ranklet transformation and another one is texture description using  
211 statistical descriptor.

212

213 (a) *Filtering with Ranklets*

214

215 In practice, ranklet transformation works with gray scale images, so images are converted into  
216 gray scale for this part. Let, each resolution contains  $N$  number of gray scale pixels. First,  
217 it is broken into two equal halves, one subset is  $T$  (treatment region) and the rest one is  $C$   
218 (control region), these pairs of subsets are being defined differently depending on the orien-  
219 tation considered. Figure 3, describes  $T$  and  $C$  for three different orientations where,  $T_V$  and  
220  $C_V$  are for vertical,  $T_H$  and  $C_H$  are for horizontal, and  $T_D$  and  $C_D$  are for diagonal orientation.

221

222 Then, non-parametric analysis is performed for each resolution and orientation. Initially,  
223 pixels of  $T$  and  $C$  regions satisfy the condition, that the gray scale value of pixels  $p_m \in T$   
224 is always higher than that of  $p_n \in C$ . Therefore, the ranklet coefficient is calculated based on  
225 the relative rank of pixels instead of their gray-scale intensity value,

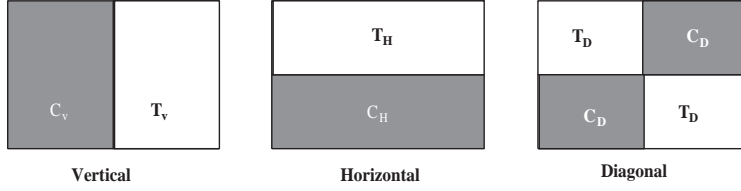


Figure 3: Different orientations of ranklet transformation.

$$R_j = \frac{\sum_{p \in T_j} \Pi(p) - \frac{N}{4} \left( \frac{N}{2} + 1 \right)}{\frac{N^2}{8}} - 1 \quad j = V, H, D \quad (4)$$

226 In (4), the summation of rank values  $\Pi(p)$  in  $T_j$  is denoted as  $\sum_{p \in T_j} \Pi(p)$ . If more squares  
 227 present in  $T_j$  that results higher intensity value than the pixels in  $C_j$ . Then the value of  
 228 ranklet coefficient  $R_j$  is inclined to +1. Contrarily, it is inclined to -1 for more number of  
 229 square crops in  $C_j$  and will have higher intensity pixel values than in  $T_j$  region. Also,  $R_V$ ,  
 230  $R_H$ , and  $R_D$  are inclined to 0, if a square contains no vertical, horizontal, and diagonal value  
 231 variation respectively. By employing this procedure, three ranklet images ( $RI$ ), i.e., for ver-  
 232 tical, horizontal, and diagonal orientations are decomposed from an image ( $I$ ). Pixel values  
 233 of these RI are represented by the ranklet coefficients  $R_V$ ,  $R_H$ , and  $R_D$  which are determined  
 234 from the square window of that specific resolution.

235

236 (b) *Statistical Descriptor*

237

238 In the proposed CRM method, each image is filtered with a set of multi-scale ranklets. There  
 239 are seven different filters are chosen for window  $W$ , where each side contains 4, 6, 8, 10,  
 240 12, 14, and 16 pixels and ranklet orientations (such as, vertical, horizontal, diagonal) are  
 241 computed for each of these resolutions. Subsequently, it takes the absolute value of filter  
 242 responses and quantizes them into 21 equally spaced bins over the interval [-1, 1].

243

244 Equations (5) and (6) are implemented to calculate the ranklet histogram ( $rhist$ ) and ranklet  
 245 co-occurrence matrix ( $rcom_{d,\theta}$ ) respectively, in order to calculate texture moments.

$$rhist(i) = \frac{n(i)}{\sum_{j=1}^{21} n(j)} \quad i = 1, \dots, 21 \quad (5)$$

246 where  $n(i)$  is the number of the  $i$ -th quantized ranklet coefficients in the RI by taking values,  
 247  $rvalue(i) = (-1, -0.9, \dots, 0, \dots, +0.9, +1)$ .

$$rcom_{d,\theta} = \frac{n_{d,\theta}(i, j)}{\sum_{l=1}^{21} \sum_{k=1}^{21} n_{d,\theta}(l, k)} \quad i, j = 1, \dots, 21 \quad (6)$$

248 The  $rcom_{d,\theta}$  converts the transitions probability between each pair of coefficients. Also,  
 249  $n_{d,\theta}(i, j)$  is the frequency of ranklet values or co-occurrences which is quantized in bin  $i, j$   
 250 at a distance  $d$  pixels along  $\theta$  direction.



251 The first two texture features are derived from the ranklet histogram  $rhist$ .

252 1. Mean Convergence ( $mc$ )

$$mc = \sum_{i=1}^{21} \frac{|rvalue(i).rhist(i) - \alpha|}{\beta} \quad (7)$$

253 where,  $\alpha$  and  $\beta$  are mean and standard deviation of ranklet coefficient respectively.

254 2. Code variance ( $cv$ )

$$cv = \sum_{i=1}^{21} (rvalue(i) - \alpha)^2 .rhist(i) \quad (8)$$

255 The remaining texture features are derived from ranklet co-occurrence matrix ( $rcom_{d,\theta}$ ), where  
256  $d$  is fixed to 1 and  $\theta \in (0^\circ, 45^\circ, 90^\circ, 135^\circ)$ .

257 3. Code entropy ( $ce$ )

$$ce = \sum_{i=1}^{21} \sum_{j=1}^{21} rcom(i, j) .\log_{10}(rcom(i, j)) \quad (9)$$

258 4. Uniformity ( $un$ )

$$un = \sum_{i=1}^{21} \sum_{j=1}^{21} rcom(i, j)^2 \quad (10)$$

259 5. First order element difference moments ( $fdm$ )

$$fdm = \sum_{i=1}^{21} \sum_{j=1}^{21} |i - j| rcom(i, j) \quad (11)$$

260 6. Second order element difference moments ( $sdm$ )

$$sdm = \sum_{i=1}^{21} \sum_{j=1}^{21} (i - j)^2 rcom(i, j) \quad (12)$$

261 7. First order inverse element difference moments ( $fidm$ )

$$fidm = \sum_{i=1}^{21} \sum_{j=1}^{21} \frac{1}{1 + |i - j|} .rcom(i, j) \quad (13)$$

262 8. Second order inverse element difference moments ( $sidm$ )

$$sidm = \sum_{i=1}^{21} \sum_{j=1}^{21} \frac{1}{1 + (i - j)^2} .rcom(i, j) \quad (14)$$

263 9. First ranklet co-occurrence matrix for energy distribution ( $edrcom_1$ )

$$edrcm_1 = \sum_{i=9}^{13} \sum_{j=9}^{13} rcom(i, j) \quad (15)$$

264 10. Second ranklet co-occurrence matrix for energy distribution ( $edrcm_2$ )

$$edrcm_2 = \sum_{i=7}^{15} \sum_{j=7}^{15} rcom(i, j) - edrcm_1 \quad (16)$$

265 11. Third ranklet co-occurrence matrix for energy distribution ( $edrcm_3$ )

$$edrcm_3 = \sum_{i=3}^{19} \sum_{j=3}^{19} rcom(i, j) - edrcm_1 - edrcm_2 \quad (17)$$

266 So, there are 231 features (from (7) to (16)) produced to represent the texture of each RI. A  
 267 top-down structuring approach of this feature extraction technique is included in Algorithm  
 268 2.

---

**Algorithm 2** Pseudo code for ranklet transformation

---

**Require:** all the pixel values are in *Gray Scale*

*Gray scale image function =  $f(x, y)$*

**for all** *resolution = 4 to 16 do*

**for all**  $x = 1$  to (*Number of rows in image* – (*resolution* – 1)) **do**

**for all**  $y = 1$  to (*Number of columns in image* – (*resolution* – 1)) **do**

*Put rank for the values of resolution*

*Break the image into T and C region*

**for all** *Orientation =  $T_{Horizontal}$ ,  $T_{Vertical}$ ,  $T_{Diagonal}$  do*

*Calculate Ranklet Coefficient R for each orientation (from, Eq. 4)*

**end for**

**Return** *Three Ranklet Images For Each Resolution*

**for all** *Ranklet Image =  $RI_{Horizontal}$ ,  $RI_{Vertical}$ ,  $RI_{Diagonal}$  do*

*Calculate Ranklet Histogram (rhist) (from Eq. 5)*

*Calculate Ranklet Co Occurrence Matrix (rcom) (from Eq. 6)*

**Then,**

*Calculate 11 texture features (using, Eq. 7 to Eq. 17)*

**end for**

**end for**

**end for**

**end for**

**Return,** *Feature vector*

---

269 *2.1.3. Moment Invariants*

270 The earliest remarkable work on moments for image processing and pattern recognition was  
 271 performed by Hu [39] and Alt [40], which is used as a shape feature extractor in the proposed  
 272 CRM algorithm. It derives relative and absolute combinations of moments from binary

273 images which are translation, rotation and scale invariant. If  $(x, y)$  is the co-ordinate of the  
 274 pixel and  $M_{p,q}$  is the 2D moment of the image function  $f(x, y)$ , then order of the moment is  
 275  $(p + q)$  where,  $p$  and  $q$  are natural numbers. Image regular moments  $M_{p,q}$  are defined as,

$$M_{p,q} = \int \int x^p y^q f(x, y) dx dy \quad (18)$$

276 Digital form of the above equation becomes,

$$M_{p,q} = \sum_x \sum_y x^p y^q f(x, y) \quad (19)$$

277 The image centroids are used to define the central moments for normalization and translation  
 278 of the image plane. The centre of gravity of the image are calculated by (18).

$$x_c = \frac{M_{10}}{M_{00}} \quad y_c = \frac{M_{01}}{M_{00}} \quad (20)$$

279 The central moments  $(\omega_{p,q})$  of order  $(p + q)$  for a shape of object  $R$  are defined as,

$$\omega_{p,q} = \sum_{(x,y) \in R} (x - x_c)^p (y - y_c)^q \quad (21)$$

280 where  $(x_c, y_c)$  is the center of that object. The ratio  $\rho_{p,q}$  is determined to make the features  
 281 scale invariant [41] as,  $\rho_{p,q} = \frac{\omega_{p,q}}{\omega_{0,0}^{(p+q+2)/2}}$ . A set of moments  $(\xi_1$  to  $\xi_7)$  are calculated which  
 282 are translation, rotation, and scale invariant and defined as follows,

$$\xi_1 = \omega_{2,0} + \omega_{0,2} \quad (22)$$

$$\xi_2 = (\omega_{2,0} - \omega_{0,2})^2 + 4\omega_{1,1}^2 \quad (23)$$

$$\xi_3 = (\omega_{3,0} - 3\omega_{1,2})^2 + (\omega_{0,3} - 3\omega_{2,1})^2 \quad (24)$$

$$\xi_4 = (\omega_{3,0} + \omega_{1,2})^2 + (\omega_{0,3} + \omega_{2,1})^2 \quad (25)$$

$$\begin{aligned} \xi_5 = & (\omega_{3,0} - 3\omega_{1,2})(\omega_{0,3} + \omega_{1,2})[(\omega_{0,3} + \omega_{1,2})^2 - 3(\omega_{0,3} + \omega_{2,1})^2] \\ & + (\omega_{0,3} - 3\omega_{2,1})(\omega_{0,3} + \omega_{2,1})[(\omega_{0,3} + \omega_{2,1})^2 - 3(\omega_{3,0} + \omega_{1,2})^2] \end{aligned} \quad (26)$$

$$\xi_6 = (\omega_{2,0} - \omega_{0,2})[(\omega_{3,0} + \omega_{1,2})^2 - (\omega_{0,3} + \omega_{2,1})^2] + 4\omega_{1,1}(\omega_{3,0} + \omega_{1,2})(\omega_{0,3} + \omega_{2,1}) \quad (27)$$

$$\xi_7 = (3\omega_{2,1} - \omega_{0,3})(\omega_{3,0} + \omega_{1,2})[(\omega_{3,0} - \omega_{1,2})^2 - 3(\omega_{0,3} + \omega_{2,1})^2] \quad (28)$$

283 Moment invariants have produced 7 invariant features with respect to translation, rotation  
 284 and scale to describe the shape of an image. The structural conventions of this feature  
 285 extraction mechanism are described in Algorithm 3.

---

**Algorithm 3** Pseudo code for moment invariants

---

**Require:** Binary image format

*Binary image function =  $f(x, y)$*

**for all**  $x = 1$  to Number of rows **do**

**for all**  $y = 1$  to Number of columns **do**

*Calculate the mass of the whole image,  $M_{00}$  (using Eq. 19)*

*Calculate the mass of the whole image towards  $x$  axis,  $M_{10}$  (using Eq. 19)*

*Calculate the mass of the whole image towards  $y$  axis,  $M_{01}$  (using Eq. 19)*

**end for**

**end for**

**Return,**  $M_{00}, M_{10}, M_{01}$

*Calculate centre of gravity of the image,  $x_c, y_c$  (using Eq. 20)*

*Calculate moment invariants,  $\xi_1$  to  $\xi_7$  (using, Eq. 22 to Eq. 28)*

**Return,** *Feature vector*

---

286 *2.2. Distance Metric*

287 Besides improved feature representation, good similarity measure (or distance metric) plays  
288 a crucial role for better retrieval performance. There are four similarity measures are in-  
289 vestigated during the experiment, namely Chi-squared test or  $X^2$  statistics [42], Manhattan  
290 distance or City block distance [43], Euclidean distance [44], and Canberra distance [45]. It  
291 is shown in Table 1 that, Euclidean distance metric yields better precision and recall than  
292 other distance measuring criteria. Therefore the Euclidean distance is chosen as similarity  
293 comparison method in the proposed CRM method. The similarity between two images with  
294  $n$  dimensional feature vector is obtained using Euclidean distance. Let,  $Q$  be the feature  
295 vector of query image and  $S$  is the feature vector of a stored image. The Euclidean distance  
296 between  $Q$  and  $S$  is denoted as  $D(Q, S)$ ,

$$D(Q, S) = \sqrt{\sum_{i=0}^{n-1} (Q_i - S_i)^2} \quad (29)$$

297 where  $Q = \{Q_0, Q_1, \dots, Q_{n-1}\}$  and  $S = \{S_0, S_1, \dots, S_{n-1}\}$ .

298 *2.3. Performance Metrics*

299 Precision and recall are well-known performance metrics in information retrieval. Precision or  
300 positive predictive value (PPV) specifies the retrieved outcomes which are relevant, whereas  
301 recall or sensitivity specifies relevant outcomes which are retrieved. Hence, high precision  
302 value means a system returns more relevant images than irrelevant ones. Conversely, high  
303 recall indicates the employed algorithm returns most of the relevant images. Here, precision  
304 ( $P_r$ ) and recall ( $R_e$ ) are defined as (30) and (31),

$$P_r = \frac{\text{Number of relevant images retrieved}}{\text{Total number of images retrieved}} \quad (30)$$

$$R_e = \frac{\text{Number of relevant images retrieved}}{\text{Total number of relevant images in the database}} \quad (31)$$

305 *2.4. Hypothesis Test*

306 Precision and recall values are measured to show the potential performance of the proposed  
307 work. In this section the statistical hypothesis test, one sample t-test is discussed to deter-  
308 mine the probability of the precision and recall sample mean truly being characteristic of the  
309 population or being a misinterpretation of the image population used in the experiment. The  
310 idea is to compare the average precision and recall obtained from the proposed method with  
311 the average precision and recall produced by existing methods over same image population.  
312 There are some assumptions to pursue the hypothetical test. Here, the experimental values  
313 are continuous interval variables and the sample of probability distribution of precision and  
314 recall values should be fitted in bell curve or normal distribution. As these quantitative values  
315 are independent, one sample t-test is appropriate for this analysis.

316

317 There are two kinds of hypothesis for this t-test i.e., null hypothesis and alternative hypothe-  
318 sis. The alternative hypothesis assumes the difference between an existing (precision or recall)  
319 mean and a proposed (precision or recall) mean is significant for same image population. On  
320 the other hand null hypothesis assumes the difference is insignificant. The goal is to measure  
321 any difference, regardless of direction, and a two-tailed hypothesis is used. If the direction of  
322 the difference between the evaluated sample mean and the comparison value matters, either  
323 an upper-tailed or lower-tailed hypothesis is used. The null hypothesis remains the same for  
324 each type of one sample t-test. The form of the hypothesis is formally defined below,

$$H_0 : \mu \leq \mu_0 \text{ vs. } H_a : \mu > \mu_0 \quad (32)$$

325 Equation (32) shows the right-tailed test performed in this work to look at the potential  
326 improvements or increment in precision and recall value, where null hypothesis, alternative  
327 hypothesis, hypothesized precision, recall mean (existing precision, recall mean), evaluated  
328 precision, recall mean are denoted by  $H_0$ ,  $H_a$ ,  $\mu_0$ , and  $\mu$  respectively. The standard one  
329 sample t-test equation is stated in (33).

$$t = \frac{\mu - \mu_0}{S/\sqrt{n}} \quad (33)$$

330 Where, t-statistic value or t-value, precision and standard deviation of precision, recall mean  
331 and sample size are signified by  $t$ ,  $S$ , and  $n$  respectively. Also, a desired significance level  
332  $\alpha = 0.05$  is assumed for accepting and rejecting the null hypothesis, where,  $t$  and  $p$  are  
333 compared to  $\alpha$  for deciding the statistical significance.

334 **3. Experiment and Result Analysis**

335 In this study, three features (color, texture, and shape) are combined to propose CRM method.  
336 The generation of feature vector is explained in previous sections, where, 9, 231, and 7 number  
337 of features are extracted by color moments, ranklet transformation, and moment invariant  
338 respectively for representing an image (both the database and query images). The ultimate  
339 feature vector,  $F$ , is formed by sequentially concatenating (9+231+7=247) all these features  
340 as represented in (34).

$$F = \{f_{color}(1), \dots, f_{color}(9), f_{texture}(1), \dots, f_{texture}(231), f_{shape}(1), \dots, f_{shape}(7)\} \quad (34)$$

341 Therefor, the performance of the proposed methodology is evaluated based on the results  
 342 produced for each query image and explained in the following section.

### 343 3.1. Parameter Fitting

344 The proposed model is a nonlinear combination of particular parameters which are fitted  
 345 by the method of successive approximations. These parameters are threshold of distance in  
 346 similarity or dissimilarity measurement, and significance level in one sample t-test. Threshold  
 347 for distance is assumed as 0.001 which means the distance between a query image and a  
 348 stored image of 0.001 or less is considered as a relevant image for that query. In case of  
 349 one sample t-test, the conventional 0.05 significance level is considered which, indicates the  
 350 probability value (p-value) of less than or equal to the significance level 0.05 would reject  
 351 the null hypothesis or accept otherwise. Therefore, above mentioned parameters should be  
 352 considered for validating the CRM model.

### 353 3.2. Data Details

354 Five different image databases, Simplicity, Corel-5K, Corel-10K, Caltech-101, and MSR (Mi-  
 355 crosoft Research) are employed for the experiment. The Simplicity database contains 1000  
 356 images with two types of resolution, either  $384 \times 256$  or  $256 \times 384$ , and 10 classes in JPEG  
 357 format. Large image varieties are present in the Corel databases e.g., animals, outdoor sports,  
 358 natural scenes etc. The Corel-5K database contains total 5000 images with 50 different im-  
 359 age categories like, fireworks, trees, waves, glasses, etc., and Corel-10K contains 10000 images  
 360 including 100 different categories like, doors, buildings, sunsets, etc. Each category contains  
 361 100 images of size  $192 \times 128$  or  $128 \times 192$  in JPEG format for both of the Corel subsets. Im-  
 362 age database Caltech-101 includes the pictures of objects with 101 categories. Each category  
 363 contains 40 to 800 images (mostly, 50). The size of each image is  $300 \times 200$  pixels. Microsoft  
 364 Research of Cambridge is created an image database ‘MSR’ for machine vision algorithms is  
 365 also utilize here. It contains 4313 high resolution images with 23 categories. The resolution  
 366 of each image is either  $640 \times 480$  or  $480 \times 640$ .

### 367 3.3. Retrieval Performance

368 Different distance measurement are investigated first and analyzed the outcomes for choosing  
 369 a suitable similarity measure for CRM. There are four similarity measures are applied in  
 370 CRM to acquire relevant images and the performance metrics are determined and listed in  
 371 Table 1.

372

Table 1: Precision and recall obtained using proposed CRM method with various distance measures.

Distance Metrics	Performance Metrics	Simplicity	Corel - 10K	Corel - 5K	Caltech - 101	MSR
Manhattan	Precision	0.3949	0.3817	0.3960	0.3766	0.3990
	Recall	0.0473	0.0458	0.0480	0.0451	0.0480
Chi Square	Precision	0.3941	0.2952	0.3820	0.2844	0.3241
	Recall	0.0473	0.0354	0.0460	0.0341	0.0389
Canberra	Precision	0.4268	0.3142	0.4140	0.3046	0.3858
	Recall	0.0512	0.0377	0.0500	0.0365	0.0463
Euclidean	Precision	0.6760	0.6744	0.6796	0.6450	0.6480
	Recall	0.0681	0.0577	0.0747	0.0645	0.0674

373 From Table 1 it is shown that the Chi-squared distance resulted the lowest precision compared  
 374 to the other distance metrics investigated. This may be due to the fact that the samples used  
 375 in the experiment are unpaired or independent data from large sample images [42], means  
 376 the set of images are taken from separate individuals. The Manhattan distance function  
 377 determines a grid like path distance between two data points. Hence, distance between two  
 378 integers is the sum of the differences in their corresponding components. Investigation using  
 379 Manhattan distance achieved improved precision values (minimum precision in Caltech  
 380 dataset is 0.3766, and maximum precision in MSR dataset is 0.3990) than Chi-squared test.  
 381

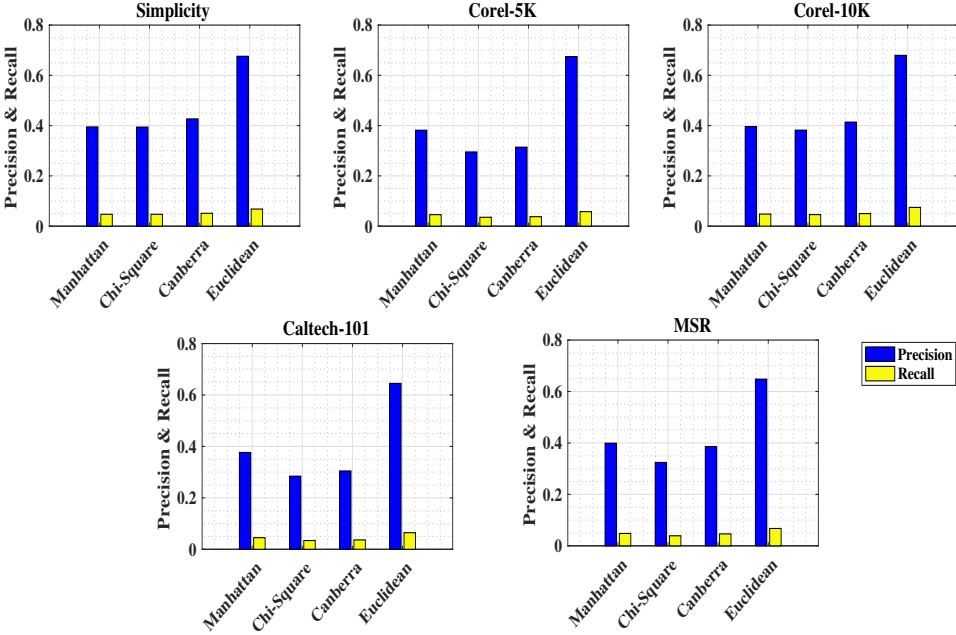


Figure 4: Performance of the proposed algorithm over different distance metrics.

382 The outcomes of Canberra distance is slightly better than Manhattan distance, yet the result  
 383 is not satisfactory, because it could produce better result when data are scattered around  
 384 origin. Here, the distinction of the absolute difference between the variables of the two images  
 385 are divided by the sum of the absolute variable values prior to summing. Euclidean  
 386 distance obtained best results among the compared distance metrics. It is obtained the minimum  
 387 distance between two sample images on a plane. Euclidean distance measures feature  
 388 wise difference of query and database images by squaring and adding the difference which,  
 389 effectively increases the divergence between them. This method also produced highest recall  
 390 compared to others, which indicates the ability of this to return more relevant results than  
 391 others. The precision and recall of the proposed CRM method are plotted in Figure 4 for  
 392 different distance metrics. This, clearly shows that, the Euclidean distance metric delivers  
 393 the better result than other metrics. Therefore, the Euclidean distance is considered for the  
 394 proposed CRM method.

395

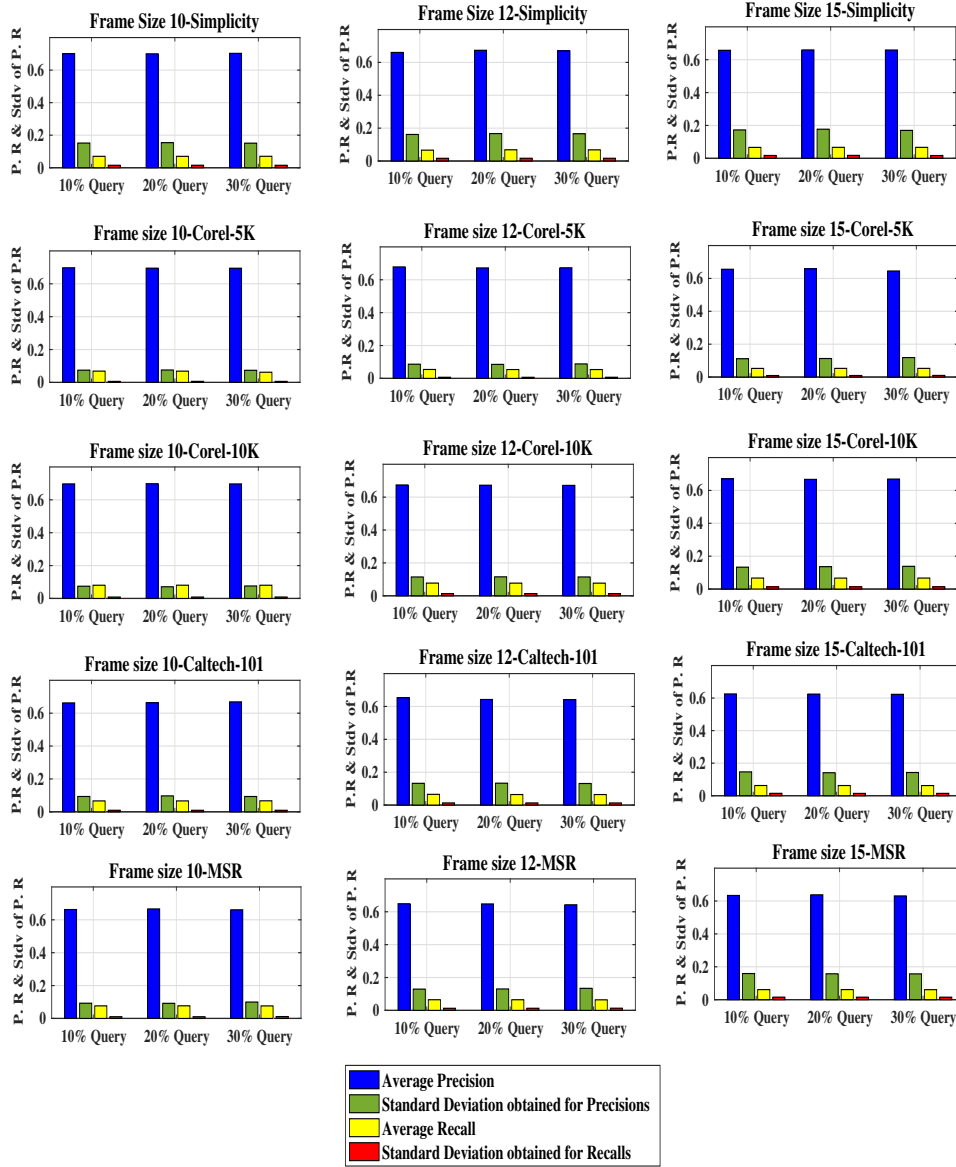


Figure 5: Average precision & recall obtained by different frame size.

396 Also, the frame size is varied by keeping distance measure (Euclidean) unchanged for investi-  
 397 gation purpose. Three frame sizes 10, 12, and 15 are employed to investigate the variation of  
 398 precision and recall when, 10%, 20%, and 30% images are selected randomly as query image  
 399 from an image database. Figure 5 shows the average precision and recall are measured for  
 400 different frame size. Along with the average precision and recall, standard deviation is also  
 401 calculated for each frame to determine the precision and recall variation. It is found that,  
 402 precision and recall are high at frame size 10, but decreased gradually for frame 12 and 15  
 403 because the misidentifications of one frame are carry forwarded by the other frames.

404



405 Table 2 encompasses the results obtained from CRM and seven recent CBIR algorithms. EHD  
406 expresses the spatial distribution of local edges for images with substantial texture which is  
407 non-homogeneous. The working procedure of this algorithm is simple. It creates histogram  
408 of edge directions for fixed size blocks. In practice, it also describes shapes depending on the  
409 edge field of object boundaries but, it is sensitive to object or scene distortions [34]. Huang et  
410 al. proposed color correlograms for image indexing and retrieval by a joint probabilistic style.  
411 Color correlogram is modified as color auto correlograms (CAC) to manage the high dimen-  
412 sionality of feature vector. Huang’s used the concept of color quantization in RGB plane to  
413 present CAC [10] which generates a 256-dimensional feature vector and apprehends spatial  
414 correlation of color intensities. It provides maximum precision 0.4977 and recall 0.0597. The  
415 obtained precision and recall are mapped in Figure 6 for comparing the performance of imple-  
416 mented algorithms visually. The plot also includes the outcomes for different image database.  
417

Table 2: Comparison of proposed CRM method with existing algorithms.

Methods	Measurements	Simplicity	Corel-5K	Corel-10K	Caltech-101	MSR
EHD	Precision	0.3721	0.4087	0.3431	0.3731	0.3817
	Recall	0.0446	0.0490	0.0411	0.0447	0.0458
CAC	Precision	0.4753	0.4977	0.3950	0.3862	0.3951
	Recall	0.0570	0.0597	0.0474	0.0463	0.0474
MTH	Precision	0.4852	0.5011	0.4157	0.4064	0.4157
	Recall	0.0582	0.0601	0.0498	0.0487	0.0498
CDH	Precision	0.5454	0.5874	0.4735	0.4629	0.4735
	Recall	0.0654	0.0704	0.0568	0.0555	0.0568
DCTon	Precision	0.5514	0.4878	0.4953	0.4350	0.4800
	Recall	0.0686	0.0616	0.0689	0.0641	0.0635
GR	Precision	0.6631	0.6319	0.6202	0.6500	0.6489
	Recall	0.0630	0.0490	0.0422	0.0580	0.0410
LDM	Precision	0.6523	0.6176	0.6437	0.6498	0.5608
	Recall	0.0618	0.0567	0.0585	0.0625	0.0540
CRM	Precision	0.6760	0.6744	0.6796	0.6450	0.6480
	Recall	0.0681	0.0577	0.0747	0.0645	0.0674

418 MTH illustrates spatial correlation of color intensities and edge orientation by employing  
419 texton analysis [19]. MTH considers four types of texton which may not depict the complete  
420 content of texton elements, because it fails to consider the perceptual uniform color differ-  
421 ence. It produced 0.4852 precision and 0.0582 recall in Simplicity, 0.5011 precision and 0.0601  
422 recall in Corel-5K, 0.4157 precision and 0.0498 recall in Corel-10K, etc. CDH [33] measures  
423 the color difference between two pixels by using Lab color space, and generates the color edge  
424 histogram of an image. However, color differences cannot be measured in RGB color space  
425 that is close to human color perception, and it generates a high dimensional feature vector.  
426 In the case of CDH, increment of equalization number of color and edge orientation may not  
427 always enhance the description power. Therefore, results may not always be satisfactory.  
428 DCTon [27], is a hybrid CBIR method which is used to compare the performance of proposed  
429 framework. DCTon extracts the inter class features using distribution of color ton with asso-  
430 ciation of dual tree complex wavelet transformation and singular value decomposition (SVD).  
431 It is a strong feature descriptor for images which, represents color and texture information.  
432 This method produces high recall value, which signifies that, it retrieves more relevant image  
433 instances. The highest precision and recall obtained by this method are 0.5514 (in Simplicity  
434 database) and 0.0689 (in Corel-10K database) respectively. This method is limited by high

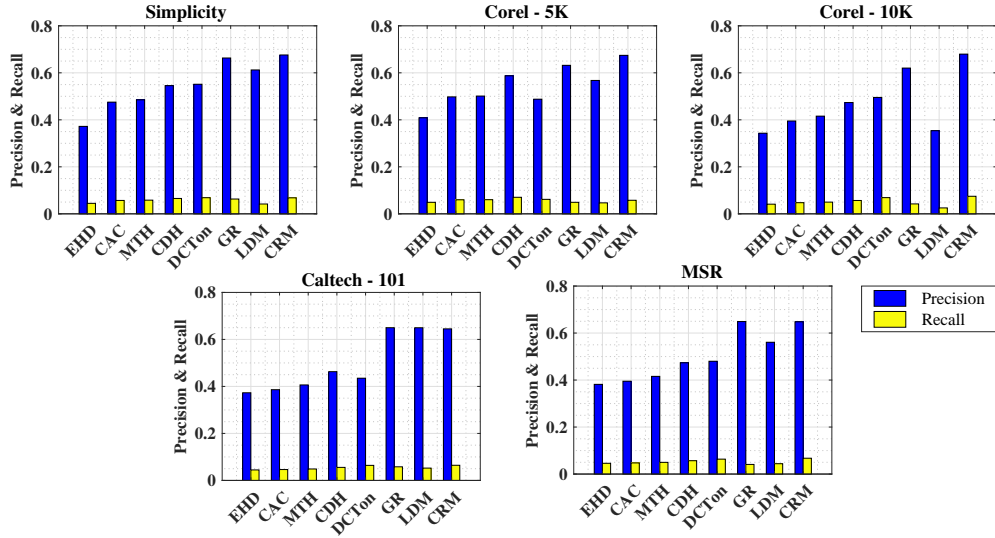


Figure 6: Performance comparison of proposed method with other existing algorithms.

435 computational complexity and scattering property of light. In [13], an indexed and encoded  
436 representation of color information is used to retrieve images from large databases. In first  
437 stage, the insignificant colors are discarded and important color information are kept to make  
438 an indexed color histogram. Then, the GR encoding is used to represent the indexed color  
439 histogram. This indexed histogram with GR encoding based CBIR method achieves good  
440 precision 0.6631 in Simplicity database. In case of Corel-5K and Corel-10K, it retrieved low  
441 amount of relevant images which results low precisions of 0.6319 and 0.6202 respectively.  
442 Also, it delivers low recall (0.0422 and 0.0410) in Corel-10K and MSR databases, which in-  
443 dicates the number of relevant images over total images is low. This GR encoding based  
444 method only considers the color information of images but in practice the images contain  
445 highly complex color, shape, texture information, and semantic content. Also, the histogram  
446 ignores shape and texture which, causes the problem to distinguish different objects having  
447 same color, e.g. black dog and black elephant. The indexing method of the histogram uses  
448 limited number of simultaneous colors per image which, is unable to describe the complex  
449 color as well as other semantic information. Though, the second phase uses a lossless GR  
450 encoding, still it again employs predicted pixel value for optimizing the representation which  
451 may obscure actual meaning of an image. Srivastava and Khare [30] proposed an algorithm  
452 LDM by combining three different feature extraction techniques. Initially, the images are  
453 converted to gray scale for different levels of decomposition and LBP extracts texture infor-  
454 mation from these decomposed elements. Finally, an orthogonal transformation LM is used  
455 to represent the images. It achieved maximum precision 0.6523 in Simplicity image database  
456 and recall 0.0625 in Caltech-101 dataset. The multi level decomposition of images causes in-  
457 tensive computational complexity, but the method shows a good set of average precision and  
458 recall. In some cases it cannot discriminate among the images. The MSR dataset contains  
459 images with complex color. However, this method uses gray scale which is a bottleneck for  
460 describing the color distribution. It may be a reason for not to produce good result in MSR.  
461 The result shows that, the method is retrieved few number of relevant images over the frames

462 as well as from each database which, causes a low precision and recall fraction. Experiment  
 463 also indicates that, this method unable to discriminate among different views of an object.

464

Query Image	Retrieved Image - 1	Retrieved Image - 2	Retrieved Image - 3
			
Retrieved Image - 4	Retrieved Image - 5	Retrieved Image - 6	Retrieved Image - 7
			
Retrieved Image - 8	Retrieved Image - 9	Retrieved Image - 10	Retrieved Image - 11
			
Retrieved Image - 12	Retrieved Image - 13	Retrieved Image - 14	Retrieved Image - 15
			

Figure 7: Picture in left top most is the query and remaining images are the retrieved ones.

465 The proposed CRM is a hybrid mechanism of three features which, increased the discrim-  
 466 ination power between images. Although the total feature vector length is 247 which, can  
 467 be considered a little high however, it reflects high discrimination power among the images.  
 468 The proposed method achieved highest precision 0.6796 and recall 0.0747 in the Corel-10K  
 469 database. The lowest precision and recall outcomes are 0.6450 and 0.0645 respectively in the  
 470 Caltech-101 database. Two examples of the retrieval result are shown in Figure 7 and Fig-  
 471 ure 8 from MSR image database. The query image of Figure 7 is a door image which is nearly  
 472 dark brown in color and rectangular in shape with texture. CRM retrieved 10 correct images

Query Image	Retrieved Image - 1	Retrieved Image - 2	Retrieved Image - 3
			
Retrieved Image - 4	Retrieved Image - 5	Retrieved Image - 6	Retrieved Image - 7
			
Retrieved Image - 8	Retrieved Image - 9	Retrieved Image - 10	Retrieved Image - 11
			
Retrieved Image - 12	Retrieved Image - 13	Retrieved Image - 14	Retrieved Image - 15
			

Figure 8: Picture in left top most is the query and remaining images are the retrieved ones.

473 out of 15. If the frame size of 10 is being considered then CRM retrieved all the relevant  
474 images but, in case of frame size 12 and 15, few irrelevant retrieval images are found. Thus,  
475 the precision 0.6666 is determined for the particular instance of frame size 15. Though, it is  
476 important that the 10 images are retrieved correctly irrespective of different color and tex-  
477 ture whereas, 5 incorrectly retrieved images are somehow homologous with respect to color,  
478 texture, and shape. In case of Figure 8, the query image is an yellow flower from a green  
479 field where, CRM return 12 relevant images among 15. Somehow, all 15 retrieved images are  
480 similar in nature because, all are flower images e.g., image 13th in the frame is visually similar  
481 but white in color. This results precision of 0.8 which is quite high. Overall, it can be stated  
482 that proposed multi-feature fusion is effective towards improvement of CBIR performance.



483 *3.4. Result Validation*

484 The precision and recall measurements illustrate the accuracy of the proposed method based  
 485 on relevant and irrelevant images are being returned for a query. The precision and recall  
 486 data are systematically examined with the purpose of highlighting useful information and  
 487 the results of this quantitative experimental work communicated via tables and graphs. The  
 488 hypothesis test is conducted to determine the impact and quality of the work presented here.  
 489 The CRM method used continuous interval variables throughout the experiment, therefore,  
 490 a quantitative inferential analysis is possible based on the probability distribution of the pre-  
 491 cision and recall samples. A sample of probability distribution of precision and recall values  
 492 for 30% query image from MSR and Caltech-101 image database are included in Figure 9,  
 493 and the data distribution curves are of bell shape or normal distribution.

494

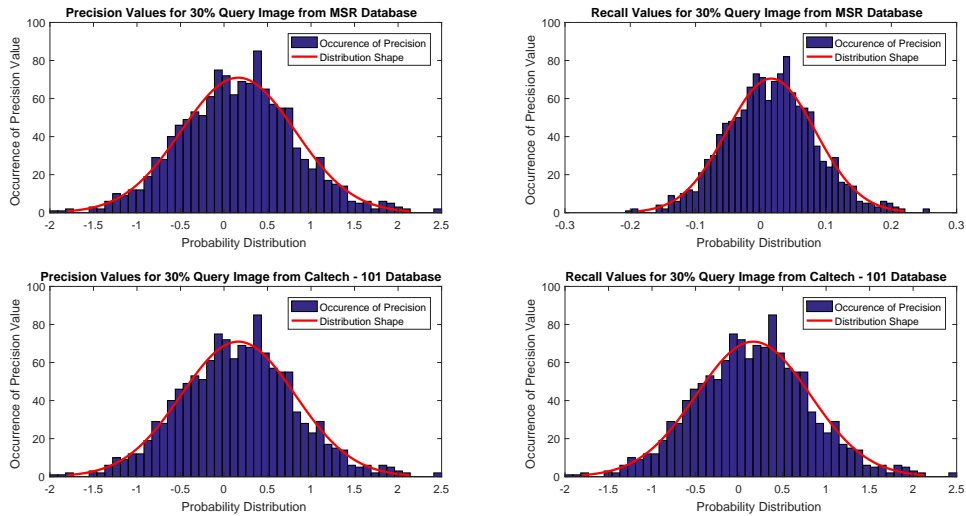


Figure 9: Distribution of precision, recall scores in MSR and Caltech-101 image database.

495 Therefore, a parametric statistical test is performed based on the shape of the curve. Ac-  
 496 cording to theoretical assumptions, normally distributed data could be tested via t-test or  
 497 t-statistic. In the proposed work, images are independent in nature, so the one sample t-test  
 498 is performed on determined precision and recall samples. The test is used to prove that, the  
 499 means of precisions and recalls are determined from the same image databases. The t-values  
 500 of precision and recall are calculated from five image databases using (33). Table 3 is in-  
 501 cluded to present the  $p$  values obtained from different image database. The t-test is executed  
 502 to established the obtained precision and recalls. These dataset are already being used by  
 503 existing algorithms, mentioned earlier. Equations (32) and (33) are used to calculate the  $p$   
 504 and  $t$  values where, precision and recall means of existing techniques (listed in Table 2) are  
 505 considered as hypothesized mean.

506 The precision and recall mean are obtained from CRM are considered as sample mean.  
 507 Sample and hypothetical means are compared to determined  $t$  and  $p$  values. The  $p$  value less  
 508 than significance level ( $\alpha$ ) and  $t$  value is conventionally considered as significant which, also  
 509 decides the acceptance and rejection of null hypothesis (described in Section 2.4). It is found

Table 3: p values from precision and recalls over different database and existing algorithms.

Methods	t-test Parameters	Simplicity	Corel-5K	Corel-10K	Caltech-101	MSR
EHD & CRM	$P_{precision}$	0.00025	0.00045	0.00037	0.00014	0.00041
	$P_{recall}$	0.00017	0.00091	0.00050	0.00088	0.00086
CAC & CRM	$P_{precision}$	0.00047	0.00029	0.00059	0.00059	0.00017
	$P_{recall}$	0.00018	0.00036	0.00011	0.00065	0.00038
MTH & CRM	$P_{precision}$	0.00083	0.00017	0.00041	0.00093	0.00044
	$P_{recall}$	0.00023	0.00088	0.00090	0.00019	0.00021
CDH & CRM	$P_{precision}$	0.00072	0.00068	0.00032	0.00018	0.00031
	$P_{recall}$	0.00067	0.00024	0.00027	0.00060	0.00086
DCTon & CRM	$P_{precision}$	0.00092	0.00038	0.00011	0.00039	0.00035
	$P_{recall}$	0.00553	0.00045	0.02170	0.00794	0.00066
GR & CRM	$P_{precision}$	0.00417	0.00059	0.00075	0.00677	0.00836
	$P_{recall}$	0.00062	0.00085	0.00016	0.00022	0.00042
LDM & CRM	$P_{precision}$	0.02370	0.00028	0.00056	0.00752	0.00074
	$P_{recall}$	0.00012	0.00060	0.00017	0.00058	0.00067

510 that the resultant  $p$  values are statistically meaningful and validate the proposed findings.  
 511 Subsequently, the  $p$  values are plotted against respective  $t$  values as shown in Figure 10. In  
 512 Figure 10, it is clearly shown that, the  $t$ -values are large and  $p$ -values are comparatively  
 513 very small which, is statistically very significant. Additionally, if  $p$ -values failed to meet the  
 514 significant threshold level  $\alpha$  ( $=0.05$ ) results the rejection of null hypothesis mentioned in  
 515 (33). The pictorial representation of null hypothesis acceptance and rejection are added in  
 516 Figure 11. This figure also indicates decreased support for the null hypothesis because, the  
 517  $p$ -values never meets the cut-off or threshold value at which statistical significance of 0.05 is  
 518 claimed, also it ensures approximately 95% of confidence in the results.

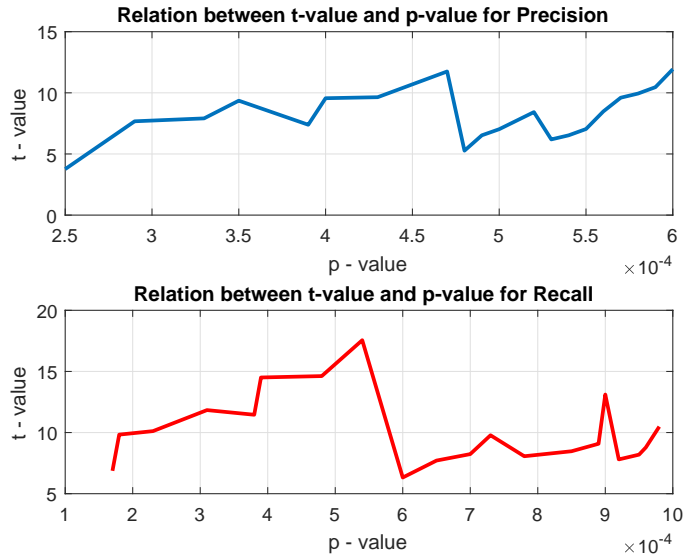


Figure 10: Relation between t-value and p-value.

### 519 3.5. Discussion

520 CBIR is a classical and difficult research domain because of the increasing image size, col-  
 521 lection, and distinct image nature. Also, the technical aspects here to represent human

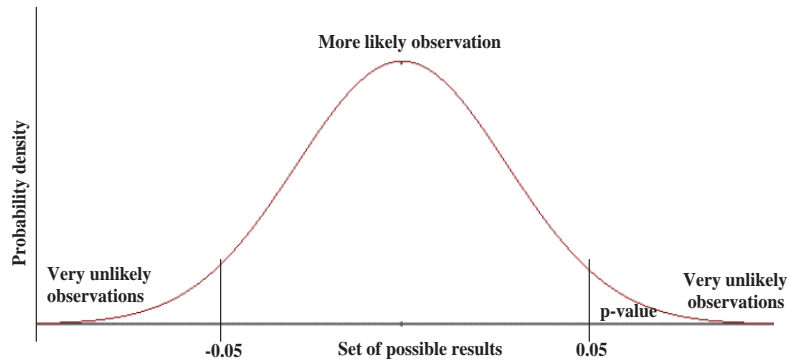


Figure 11: Null hypothesis acceptance and rejection.

522 perception makes this domain complex. Despite of the rich state-of-art, the real-time image  
 523 retrieval is quite challenging due to the diverse image property. For example, Figure  
 524 7 includes the 15 retrieved images for single query image of door. The different doors have  
 525 different properties due to the image contrast or color or the time when the picture was taken  
 526 or the camera resolution or many more. Visually, it can be seen that, shape and texture are  
 527 dominant feature here because, user needs the doors of any color and doors are always same  
 528 in size. In Figure 8, user needs a yellow flower which has its own shape. Hence, the color  
 529 and shape are dominant in this case. So, the proposed study tried to provide an efficient  
 530 and hybrid CBIR approach that, doesn't lose any significant property of an image and re-  
 531 trieve relevant images as much as possible. Thus, the selection of different feature extraction  
 532 algorithms is vital step towards the CBIR process. Color moment, ranklet transformation,  
 533 and moment invariant are selected to make an efficient CBIR tool by using their individual  
 534 capabilities. Also, the other aspects of CBIR such as, similarity measure and performance  
 535 analysis over different frame size (10, 12, and 15) are explored to tune the performance prop-  
 536 erly where, Euclidean measure delivers optimal performance for all the relevant image search.  
 537 The proposed method is executed over five different image dataset and compared with re-  
 538 cent CBIR techniques. This comparison assure the performance of this method is prevailing  
 539 among other method across all the five database images. Eventually, the one sample t-test  
 540 is executed to validate the work theoretically and practically.

#### 541 4. Conclusion & Future work

542 The proposed CRM method combines three invariant features which is implemented over  
 543 five different image databases and achieved significant precision values with respect to other  
 544 existing techniques. Experimental result shows that, this is a good representation of images,  
 545 and generates very high discrimination power among images. CRM uses the feature vector  
 546 of length 247, which is comparatively high with respect to other existing techniques may  
 547 cause of longer time complexity. Thus, reduction of feature vector length would be a future  
 548 consideration as time is also a pivotal property of CBIR systems. Another issue that would  
 549 be taken into account is the purification of obtained results by using relevance feedback (RF).  
 550 The results that are initially returned for a given query would be visually filtered through  
 551 human intervention and put the feedback to system for better results in the next iteration.

552 **References**

- 553 [1] C. H. Chuang, S. C. Cheng, C. C. Chang, Y. P. P. Chen, Model-based approach to  
554 spatial-temporal sampling of video clips for video object detection by classification,  
555 *Journal of Visual Communication and Image Representation* 25 (2014) 1018–1030.
- 556 [2] H. T. Wu, J. Huang, Y. Q. Shi, A reversible data hiding method with contrast enhance-  
557 ment for medical images, *Journal of Visual Communication and Image Representation*  
558 31 (2015) 146–153.
- 559 [3] M. Gouiffès, B. Planes, C. Jacquemin, HTRI: High time range imaging, *Journal of*  
560 *Visual Communication and Image Representation* 24 (2013) 361–372.
- 561 [4] W. Xing Yuan, L. Fan Ping, W. Shu Guo, Fractal image compression based on spatial  
562 correlation and hybrid genetic algorithm, *Journal of Visual Communication and Image*  
563 *Representation* 20 (2009) 505–510.
- 564 [5] I. K. Sethi, I. L. Coman, D. Stan, Mining association rules between low-level image  
565 features and high-level concepts, in: *Data Mining and Knowledge Discovery: Theory,*  
566 *Tools, and Technology III*, International Society for Optics and Photonics, Orlando, FL,  
567 United States (2001), pp. 279–291.
- 568 [6] C. H. Lin, R. T. Chen, Y. K. Chan, A smart content-based image retrieval system based  
569 on color and texture feature, *Image and Vision Computing* 27 (2009) 658–665.
- 570 [7] Y. Liu, D. Zhang, G. Lu, W.-Y. Ma, A survey of content-based image retrieval with  
571 high-level semantics, *Pattern recognition* 40 (2007) 262–282.
- 572 [8] R. Weber, M. Mlivonic, Efficient region-based image retrieval, in: *Proceedings of*  
573 *the twelfth international conference on Information and knowledge management*, New  
574 Orleans, LA, USA (2003), pp. 69–76.
- 575 [9] S. H. Schwartz, *Visual Perception: A Clinical Orientation*, 3rd edition, 2004.
- 576 [10] J. Huang, S. R. Kumar, M. Mitra, W. J. Zhu, R. Zabih, Image indexing using color  
577 correlograms, in: *Proceedings of the IEEE Computer Society Conference on Computer*  
578 *Vision and Pattern Recognition*, Washington, DC, United States (1997), pp. 762–768.
- 579 [11] B. S. Manjunath, J. R. Ohm, V. V. Vasudevan, A. Yamada, Color and texture de-  
580 scriptors, *IEEE Transactions on Circuits and Systems for Video Technology* 11 (2001)  
581 703–715.
- 582 [12] B. S. Manjunath, P. Salembier, T. Sikora, *Introduction to MPEG-7: Multimedia Content*  
583 *Description Interface*, John Wiley & Sons, Inc., New York, NY, USA, 2002.
- 584 [13] S. Shaila, A. Vadivel, Indexing and encoding based image feature representation with bin  
585 overlapped similarity measure for cbir applications, *Journal of Visual Communication*  
586 *and Image Representation* 36 (2016) 40–55.
- 587 [14] R. M. Haralick, K. Shanmugam, Dinstein, Textural features for image classification,  
588 *IEEE Transactions on Systems, Man and Cybernetics SMC-3* (1973) 610–621.



- 589 [15] H. Tamura, S. Mori, T. Yamawaki, Textural features corresponding to visual perception,  
590 IEEE Transactions on Systems, Man and Cybernetics 8 (1978) 460–473.
- 591 [16] G. R. Cross, A. K. Jain, Markov random field texture models, IEEE Transactions  
592 Pattern Analysis and Machine Intelligence 5 (1983) 25–39.
- 593 [17] B. S. Manjunath, W. Y. Ma, Texture features for browsing and retrieval of image data,  
594 IEEE Transactions on Pattern Analysis and Machine Intelligence 18 (1996) 837–842.
- 595 [18] T. Ojala, M. Pietikainen, T. Maenpaa, Multiresolution gray-scale and rotation invariant  
596 texture classification with local binary patterns, IEEE Transactions on Pattern Analysis  
597 and Machine Intelligence 24 (2002) 971–987.
- 598 [19] G. H. Liu, L. Zhang, Y. K. Hou, Z. Y. Li, J. Y. Yang, Image retrieval based on multi-  
599 texton histogram, Pattern Recognition 43 (2010) 2380–2389.
- 600 [20] G. H. Liu, J. Y. Yang, Image retrieval based on the texton co-occurrence matrix, Pattern  
601 Recognition 41 (2008) 3521–3527.
- 602 [21] G. H. Liu, Z. Y. Li, L. Zhang, Y. Xu, Image retrieval based on micro-structure descriptor,  
603 Pattern Recognition 44 (2011) 2123 – 2133.
- 604 [22] J. Luo, D. J. Crandall, Color object detection using spatial-color joint probability func-  
605 tions., IEEE Transactions on Image Processing 15 (2006) 1443–1453.
- 606 [23] W. Burger, M. J. Burge, Principles of Digital Image Processing: Core Algorithms,  
607 Springer Publishing Company, Incorporated, 1st edition, 2009.
- 608 [24] R. C. Gonzalez, R. E. Woods, Digital Image Processing, Prentice-Hall, Inc., Upper  
609 Saddle River, NJ, USA, 3rd edition, 2006.
- 610 [25] D. G. Lowe, Distinctive image features from scale-invariant keypoints, International  
611 Journal of Computer Vision 60 (2004) 91–110.
- 612 [26] J. C. V. Gemert, C. J. Veenman, A. W. M. Smeulders, J. M. Geusebroek, Visual word  
613 ambiguity, IEEE Transactions on Pattern Analysis and Machine Intelligence 32 (2010)  
614 1271–1283.
- 615 [27] M. Rahimi, M. E. Moghaddam, A content-based image retrieval system based on color  
616 ton distribution descriptors, Signal, Image and Video Processing 9 (2015) 691–704.
- 617 [28] L. Feng, J. Wu, S. Liu, H. Zhang, Global correlation descriptor: a novel image represen-  
618 tation for image retrieval, Journal of Visual Communication and Image Representation  
619 33 (2015) 104–114.
- 620 [29] M. Zhao, H. Zhang, J. Sun, A novel image retrieval method based on multi-trend  
621 structure descriptor, Journal of Visual Communication and Image Representation 38  
622 (2016) 73–81.
- 623 [30] P. Srivastava, A. Khare, Integration of wavelet transform, local binary patterns and  
624 moments for content-based image retrieval, Journal of Visual Communication and Image  
625 Representation 42 (2017) 78–103.

- 626 [31] C. Cui, P. Lin, X. Nie, Y. Yin, Q. Zhu, Hybrid textual-visual relevance learning for  
627 content-based image retrieval, *Journal of Visual Communication and Image Representa-*  
628 *tion* (2017).
- 629 [32] V. Kim, L. Iaroslavskii, Rank algorithms for picture processing, *Computer Vision*  
630 *graphics and image processing* 35 (1986) 234–258.
- 631 [33] G. H. Liu, J. Y. Yang, Content-based image retrieval using color difference histogram,  
632 *Pattern Recognition* 46 (2013) 188–198.
- 633 [34] C. S. Won, D. K. Park, S.-J. Park, Efficient use of MPEG-7 edge histogram descriptor,  
634 *ETRI journal* 24 (2002) 23–30.
- 635 [35] J. D. Foley, A. V. Dam, S. K. Feiner, J. F. Hughes, *Computer Graphics: Principles and*  
636 *Practice* (2nd Ed.), Addison-Wesley Longman Publishing Co., Inc., Boston, MA, USA,  
637 1990.
- 638 [36] M. A. Stricker, M. Orengo, Similarity of color images, in: *Storage and Retrieval for*  
639 *Image and Video Databases III*, International Society for Optics and Photonics, San  
640 Jose, CA, United States (1995), pp. 381–393.
- 641 [37] Texture classification using invariant ranklet features, *Pattern Recognition Letters* 29  
642 (2008) 1980–1986.
- 643 [38] R. Hodgson, D. Bailey, M. Naylor, A. Ng, S. McNeill, Properties, implementations and  
644 applications of rank filters, *Image and Vision Computing* 3 (1985) 3–14.
- 645 [39] M. K. Hu, Visual problem recognition by moment invariants, *IRE Transactions on*  
646 *Information Theory IT-8* (1962) 179–187.
- 647 [40] F. L. Alt, Digital pattern recognition by moments, *Journal of the ACM (JACM)* 9  
648 (1962) 240–258.
- 649 [41] A. K. Jain, F. Farrokhnia, Unsupervised texture segmentation using gabor filters, *Pat-*  
650 *tern recognition* 24 (1991) 1167–1186.
- 651 [42] N. K. G. Gosall, G. Singh, *Doctor’s Guide to Critical Appraisal* (3 Ed.), Knutsford:  
652 PasTest, 2012.
- 653 [43] D. L. Donoho, For most large underdetermined systems of linear equations the minimal  
654  $l_1$ -norm solution is also the sparsest solution, *Communications on Pure and Applied*  
655 *Mathematics* 59 (2006) 797–829.
- 656 [44] W. Ma, B. S. Manjunath, Netra: A toolbox for navigating large image databases,  
657 *Multimedia systems* 7 (1999) 184–198.
- 658 [45] G. N. Lance, W. T. Williams, Computer programs for hierarchical polythetic classifica-  
659 tion (“similarity analysis”), *The Computer Journal* 9 (1966) 60–64.